

1  
2  
3  
4  
5  
6

**Original Research Article**  
**MHD Free Convection, Heat and Mass Transfer  
Chemical Reaction, Radiation and Heat Source  
or Sink over a Rotating Inclined Permeable  
Plate Variable Reactive Index**

7  
8  
9  
10

---

---

**ABSTRACT**

MHD free convection, heat and mass transfer flow over a rotating inclined permeable plate with the influence of magnetic field, thermal radiation and chemical reaction of various order has been investigated numerically. The governing boundary-layer equations are formulated and transformed into a set of similarity equations with the help of similarity variables derived by lie group transformation. The governing equations are solved numerically using the Nactsheim-Swigert Shooting iteration technique together with the Runge-Kutta six order iteration schemes. The simulation results are presented graphically to illustrate influence of magnetic parameter ( $M$ ), porosity parameter ( $\gamma$ ), rotational parameter ( $R'$ ), Grashof number ( $G_r$ ), modified Grashof number ( $G_m$ ), thermal conductivity parameter ( $T_c$ ), Prandtl number ( $P_r$ ), radiation parameter ( $R$ ), heat source parameter ( $Q$ ), Eckert number ( $E_c$ ), Schmidt number ( $S_c$ ), reaction parameter ( $\lambda$ ) and order of chemical reaction ( $n$ ) on the all fluid velocity components, temperature and concentration distribution as well as Skin-friction coefficient, Nusselt and Sherwood number at the plate.

11  
12  
13

*Keywords: MHD; Inclined permeable plate; Thermal radiation; Chemical reaction;*

14  
15

**NOMENCLATURE**

16  
17  
18  
19  
20  
21  
22  
23  
24  
25

$B_0$	Constant magnetic flux density
$c$	Constant depends on the properties of the fluid
$C$	Concentration of the fluid
$C_p$	Specific heat at constant pressure
$D_m$	Mass diffusivity
$f'$	Dimensionless primary velocity
$g$	Acceleration due to gravity
$g_0$	Dimensionless secondary velocity
$k$	Thermal conductivity
$k_\infty$	Undisturbed thermal conductivity

26	$k_0$	Reaction rate
27	$K$	Permeability of the porous medium
28	$n$	Order of chemical reaction
29	$P$	Pressure distribution in the boundary layer
30	$q_r$	Radiative heat flux in the $y$ direction
31	$Q_T$	Heat generation
32	$Q_0$	Heat source
33	$t$	Time
34	$T$	Fluid temperature
35	$U$	Uniform velocity
36	$u, v$	Velocity components along $x$ and $y$ axes respectively
37	$x'$	Dimensionless axial distance along $x$ axis

38 **Dimensionless parameters**

39	$E_c$	Eckert number
40	$R'$	Rotational parameter
41	$G_r$	Grashof number
42	$G_m$	Modified Grashof number
43	$M$	Magnetic parameter
44	$P_r$	Prandtl number
45	$Q$	Heat source parameter
46	$R$	Radiation parameter
47	$S_c$	Schmidt number
48	$T_c$	Thermal conductivity parameter
49	$\gamma$	Permeability of the porous medium
50	$\lambda$	Reaction parameter

51

52 **Greek Symbols**

53	$\nu$	Kinematic viscosity of the fluid
54	$\mu$	Dynamic viscosity of the fluid
55	$\sigma$	Electrical conductivity

56	$\sigma_0$	Constant electrical conductivity
57	$\sigma_s$	Stefan-Boltzmann constant
58	$\rho$	Density of the fluid
59	$\alpha$	Thermal diffusivity
60	$\alpha_1 - \alpha_6$	Arbitrary real number
61	$\beta$	Inclination angle
62	$\beta_T$	Thermal expansion coefficient
63	$\beta_C$	Concentration expansion coefficient
64	$\kappa^*$	Mean absorption coefficient
65	$\varepsilon$	Parameter of the group
66	$\psi$	Stream function
67	$\eta$	Similarity variable
68	$\theta$	Dimensionless temperature
69	$\phi$	Dimensionless concentration
70	$\Omega$	Angular velocity of the plate
71	<b>Subscripts</b>	
72	w	Condition of the wall
73	$\infty$	Condition of the free steam

74

## 75 1. INTRODUCTION

76

77 Coupled heat and mass transfer problems in the presence of chemical reactions are of  
78 importance in many processes and have, therefore, received considerable amount of  
79 attention of researchers in recent years. Chemical reactions can occur in processes such as  
80 drying, distribution of temperature and moisture over agricultural fields and groves of fruit  
81 trees, damage of crops due to freezing, evaporation at the surface of a water body, energy  
82 transfer in a wet cooling tower and flow in a desert cooler. Chemical reactions are classified  
83 as either homogeneous or heterogeneous processes. A homogeneous reaction is one that  
84 occurs uniformly throughout a given phase. On the other hand, a heterogeneous reaction  
85 takes a restricted area or within the boundary of a phase. Analysis of the transport  
86 processes and their interaction with chemical reactions is quite difficult and closely related to  
87 fluid dynamics. Chemical reaction effects on heat and mass transfer has been analyzed by  
88 many researchers over various geometries with various boundary conditions in porous and  
89 nonporous media. Symmetry groups or simply symmetries are invariant transformations that  
90 do not alter the structural form of the equation under investigation which is described by  
91 Bluman and Kumei [1]. MHD boundary layer equations for power law fluids with variable  
92 electric conductivity is studied by Helmy [2]. In the case of a scaling group of  
93 transformations, the group-invariant solutions are nothing but the well known similarity  
94 solutions which is studied by Pakdemirli and Yurusoy [3]. Symmetry groups and similarity

95 solutions for free convective boundary-layer problem was studied by Kalpakides and  
96 Balassas [4]. Makinde [5] investigated the effect of free convection flow with thermal  
97 radiation and mass transfer past moving vertical porous plate. Seddeek and Salem [6]  
98 investigated the Laminar mixed convection adjacent to vertical continuously stretching sheet  
99 with variable viscosity and variable thermal diffusivity. Ibrahim, Elaiw and Bakr [7] studied the  
100 effect of the chemical reaction and radiation absorption on the unsteady MHD free  
101 convection flow past a semi infinite vertical permeable moving plate with heat source and  
102 suction. El-Kabeir, El-Hakiem and Rashad [8] studied Lie group analysis of unsteady MHD  
103 three dimensional dimensional by natural convection from an inclined stretching surface  
104 saturated porous medium. Rajeswari, Jothiram and Nelson [9] studied the effect of chemical  
105 reaction, heat and mass transfer on nonlinear MHD boundary layer flow through a vertical  
106 porous surface in the presence of suction. Chandrakala [10] investigated chemical reaction  
107 effects on MHD flow past an impulsively started semi-infinite vertical plate. Joneidi,  
108 Domairry and Babaelahi [11] studied analytical treatment of MHD free convective flow and  
109 mass transfer over a stretching sheet with chemical reaction. Muhaimin, Kandasamy and  
110 Hashim [12] studied the effect of chemical reaction, heat and mass transfer on nonlinear  
111 boundary layer past a porous shrinking sheet in the presence of suction. Rahman and  
112 Salahuddin [13] studied hydromagnetic heat and mass transfer flow over an inclined heated  
113 surface with variable viscosity and electric conductivity. As per standard text and works of  
114 previous researchers, the radiative flow of an electrically conducting fluid and heat and mass  
115 transfer situation arises in many practical applications such as in electrical power generation,  
116 astrophysical flows, solar power technology, space vehicle re-entry, nuclear reactors.

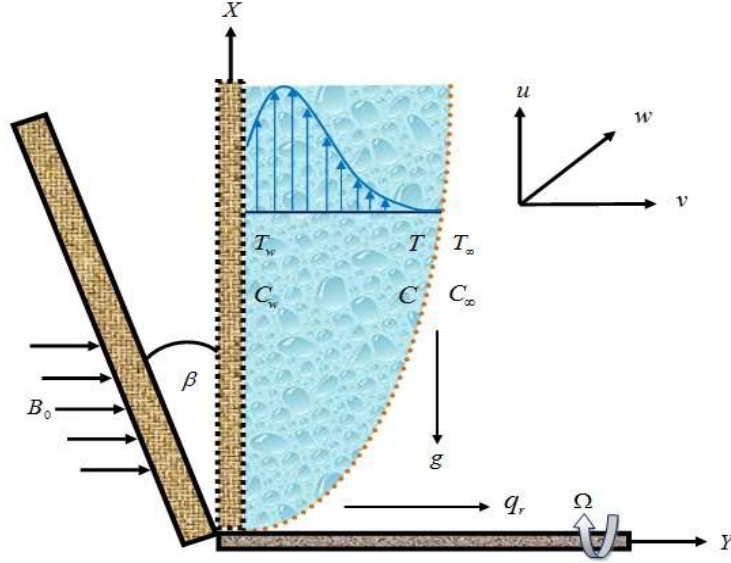
117  
118 The objective of this study is to present a similarity analysis of boundary layer flow past a  
119 rotating inclined permeable plate with the influence of magnetic field, thermal radiation,  
120 thermal conductivity and chemical reaction of various orders.

121

## 122 **2. MATHEMATICAL MODEL OF THE FLOW AND GOVERNING EQUATIONS**

123

124 Steady two dimensional MHD heat and mass transfer flow with chemical reaction and  
125 radiation over an inclined permeable plate  $y = 0$  in a rotating system under the influence of  
126 transversely applied magnetic field is considered. The  $x$ -axis is taken in the upward direction  
127 and  $y$ -axis is normal to it. Again the plate is inclined at an angle  $\beta$  with the  $x$ -axis. The flow  
128 takes place at  $y \geq 0$ , where  $y$  is the coordinate measured normal to the  $x$ -axis. Initially we  
129 consider the plate as well as the fluid is at rest with the same velocity  $U (= U_\infty)$ , temperature  
130  $T (= T_\infty)$  and concentration  $C (= C_\infty)$ . Also it is assumed that the fluid and plate is at rest  
131 after that the whole system is allowed to rotate with a constant angular velocity  
132  $R = (0, -\Omega, 0)$  about the  $y$ -axis and then the temperature and species concentration of the  
133 plate are raised to  $T_w (> T_\infty)$  and  $C_w (> C_\infty)$  respectively, which are thereafter maintained  
134 constant, where  $T_w$  and  $C_w$  is the temperature and concentration respectively at wall and  
135  $T_\infty$  and  $C_\infty$  is the temperature and concentration respectively far away from the plate.



136  
137

138 **Fig. 1. Physical configuration of the flow**

139 The electrical conductivity is assumed to vary with the velocity of the fluid and have the form  
140 [2],

141  $\sigma = \sigma_0 u$ ,  $\sigma_0$  is the constant electrical conductivity.

142 The applied magnetic field strength is considered, as follows [13]

$$143 \quad B(x) = \frac{B_0}{\sqrt{x}}$$

144 The temperature dependent thermal conductivity is assumed to vary linearly, as follows [6]

$$145 \quad k(T) = k_\infty [1 + c(T - T_\infty)]$$

146 Where  $k_\infty$  is the undisturbed thermal conductivity and  $c$  is the constant depending on the  
147 properties of the fluid.

148 The governing equations for the continuity, momentum, energy and concentration in laminar  
149 MHD incompressible boundary-layer flow is presented follows

$$150 \quad \frac{\partial u}{\partial x} + \frac{\partial v}{\partial y} = 0 \quad (1)$$

$$151 \quad u \frac{\partial u}{\partial x} + v \frac{\partial u}{\partial y} = \nu \frac{\partial^2 u}{\partial y^2} + 2\Omega w - \frac{\nu}{K} u - \frac{\sigma_0 B_0^2 u^2}{\rho x} + g\beta_T (T - T_\infty) \cos\beta + g\beta_C (C - C_\infty) \cos\beta \quad (2)$$

$$152 \quad u \frac{\partial w}{\partial x} + v \frac{\partial w}{\partial y} = \nu \frac{\partial^2 w}{\partial y^2} - 2\Omega u - \frac{\nu}{K} w - \frac{\sigma_0 B_0^2 u w}{\rho x} \quad (3)$$

$$153 \quad u \frac{\partial T}{\partial x} + v \frac{\partial T}{\partial y} = \frac{1}{\rho C_p} \frac{\partial}{\partial y} \left[ k(T) \frac{\partial T}{\partial y} \right] + \frac{Q_0 (T - T_\infty)}{\rho C_p} - \frac{\alpha}{k_\infty} \left( \frac{\partial q_r}{\partial y} \right) + \frac{\nu}{C_p} \left( \frac{\partial u}{\partial y} \right)^2 \quad (4)$$

$$154 \quad u \frac{\partial C}{\partial x} + v \frac{\partial C}{\partial y} = D_m \frac{\partial^2 C}{\partial y^2} - k_0 (C - C_\infty)^n \quad (5)$$

155 and the boundary conditions for the model is

$$156 \quad \left. \begin{aligned} u = U, v = 0, w = 0, T = T_w, C = C_w \text{ at } y = 0 \\ u \rightarrow 0, w \rightarrow 0, T \rightarrow T_\infty, C \rightarrow C_\infty \text{ as } y \rightarrow \infty \end{aligned} \right\} \quad (6)$$

157 where,  $U$  is the uniform velocity,  $\beta$  is the inclination angle of the plate with  $x$ -axis,  $C_p$  is the  
 158 specific heat at constant pressure,  $k(T)$  is the temperature dependent thermal conductivity,  
 159  $Q_0$  is the heat source,  $D_m$  is the mass diffusivity,  $k_0$  is the reaction rate,  $k_0 > 0$  for destructive  
 160 reaction,  $k_0 = 0$  for no reaction and  $k_0 < 0$  for generative reaction,  $n$  (integer) is the order of  
 161 chemical reaction,  $q_r$  is the chemical reaction parameter,  $T_w$  and  $C_w$  is the temperature and  
 162 concentration respectively at wall and  $T_\infty$  and  $C_\infty$  is the temperature and concentration  
 163 respectively far away from the plate.

## 164 2.1 METHOD OF SOLUTION

165 Introducing the following dimensionless variables

$$166 \quad x' = \frac{xU}{\nu}, y' = \frac{yU}{\nu}, u' = \frac{u}{U}, v' = \frac{v}{U}, w' = \frac{w}{U}, \theta = \frac{T - T_\infty}{T_w - T_\infty} \text{ and } \phi = \frac{C - C_\infty}{C_w - C_\infty}$$

167 the following equations are obtained,

$$170 \quad u = U u', v = U v', w = U w', T = T_\infty + (T_w - T_\infty) \theta \text{ and } C = C_\infty + (C_w - C_\infty) \phi \quad (7)$$

171 Now, by using equation (7), the equations (1), (2), (3), (4) and (5) are transformed to

$$172 \quad \frac{\partial u'}{\partial x'} + \frac{\partial v'}{\partial y'} = 0 \quad (8)$$

$$173 \quad u' \frac{\partial u'}{\partial x'} + v' \frac{\partial u'}{\partial y'} = \frac{\partial^2 u'}{\partial y'^2} + 2R' w' - \gamma u' - \frac{M u'^2}{x'} + G_r \theta \cos \beta + G_m \phi \cos \beta \quad (9)$$

$$174 \quad u' \frac{\partial w'}{\partial x'} + v' \frac{\partial w'}{\partial y'} = \frac{\partial^2 w'}{\partial y'^2} - 2R' u' - \gamma w' - \frac{M u' w'}{x'} \quad (10)$$

$$175 \quad u' \frac{\partial \theta}{\partial x'} + v' \frac{\partial \theta}{\partial y'} - \frac{1}{P_r} \left[ (1 + T_c \theta + R) \frac{\partial^2 \theta}{\partial y'^2} + T_c \left( \frac{\partial \theta}{\partial y'} \right)^2 \right] - Q \theta - E_c \left( \frac{\partial u}{\partial y} \right)^2 = 0 \quad (11)$$

$$176 \quad u' \frac{\partial \phi}{\partial x'} + v' \frac{\partial \phi}{\partial y'} - \frac{1}{S_c} \frac{\partial^2 \phi}{\partial y'^2} + \lambda \phi^n = 0 \quad (12)$$

177 using equation (7), the boundary condition (6) becomes,

$$178 \quad \left. \begin{aligned} u' = 1, v' = 0, w' = 0, \theta = 1, \phi = 1 \text{ at } y' = 0 \\ u' \rightarrow 0, w' \rightarrow 0, \theta \rightarrow 0, \phi \rightarrow 0 \text{ as } y' \rightarrow \infty \end{aligned} \right\} \quad (13)$$

179 where,

$$180 \quad R' = \frac{\Omega \nu}{U^2}, \gamma = \frac{\nu^2}{KU^2}, M = \frac{\sigma_0 B_0^2}{\rho}, G_r = \frac{g \beta_T (T_w - T_\infty) \nu}{U^3}, G_m = \frac{g \beta_c (C_w - C_\infty) \nu}{U^3}, T_c = c(T_w - T_\infty),$$

$$181 \quad R = \frac{16 \sigma_s T_\infty^3}{3 \kappa^* k_\infty}, P_r = \frac{\nu}{\alpha}, Q = \frac{Q_0 \nu}{\rho C_p U^2}, E_c = \frac{U^2}{C_p (T_w - T_\infty)}, S_c = \frac{\nu}{D_m} \text{ and } \lambda = \frac{k_0 (C_w - C_\infty)^{n-1} \nu}{U^2}$$

182 In order to deal with the problem, we introduce the stream function  $\psi$  (since the flow is  
183 incompressible) defined by

$$184 \quad u' = \frac{\partial \psi}{\partial y'}, v' = -\frac{\partial \psi}{\partial x'} \quad (14)$$

185 The mathematical significance of using equation (14) is that the continuity equation (8) is  
186 satisfied automatically.

187 by equation (14), equations (9), (10), (11) and (12) transformed as follows,

$$188 \quad \frac{\partial \psi}{\partial y'} \frac{\partial^2 \psi}{\partial x' \partial y'} - \frac{\partial \psi}{\partial x'} \frac{\partial^2 \psi}{\partial y'^2} - \frac{\partial^3 \psi}{\partial y'^3} - 2R'w' + \gamma \frac{\partial \psi}{\partial y'} + \frac{M}{x'} \left( \frac{\partial \psi}{\partial y'} \right)^2 - G_r \theta \cos \beta - G_m \phi \cos \beta = 0 \quad (15)$$

$$189 \quad \frac{\partial \psi}{\partial y'} \frac{\partial w'}{\partial x'} - \frac{\partial \psi}{\partial x'} \frac{\partial w'}{\partial y'} - \frac{\partial^2 w'}{\partial y'^2} + 2R' \frac{\partial \psi}{\partial y'} + \gamma w' + \frac{M}{x'} \frac{\partial \psi}{\partial y'} w' = 0 \quad (16)$$

$$190 \quad \frac{\partial \psi}{\partial y'} \frac{\partial \theta}{\partial x'} - \frac{\partial \psi}{\partial x'} \frac{\partial \theta}{\partial y'} - \frac{1}{P_r} \left[ (1 + T_c \theta + R) \frac{\partial^2 \theta}{\partial y'^2} + T_c \left( \frac{\partial \theta}{\partial y'} \right)^2 \right] - Q\theta - E_c \left( \frac{\partial^2 \psi}{\partial y'^2} \right)^2 = 0 \quad (17)$$

$$191 \quad \frac{\partial \psi}{\partial y'} \frac{\partial \phi}{\partial x'} - \frac{\partial \psi}{\partial x'} \frac{\partial \phi}{\partial y'} - \frac{1}{S_c} \frac{\partial^2 \phi}{\partial y'^2} + \lambda \phi^n = 0 \quad (18)$$

192 and the boundary conditions (13) become,

$$193 \quad \left. \begin{aligned} \frac{\partial \psi}{\partial y'} = 1, \frac{\partial \psi}{\partial x'} = 0, w' = 0, \theta = 1, \phi = 1 \text{ at } y' = 0 \\ \frac{\partial \psi}{\partial y'} \rightarrow 0, w' \rightarrow 0, \theta \rightarrow 0, \phi \rightarrow 0 \text{ as } y' \rightarrow \infty \end{aligned} \right\} \quad (19)$$

194 Finding the similarity solution of the equations (15) to (18) is equivalent to determining the  
195 invariant solutions of these equations under a particular continuous one parameter group.  
196 Introducing the simplified form of Lie-group transformations [8] namely, the scaling group of  
197 transformations

$$198 \quad G_1: x^* = x'e^{\varepsilon\alpha_1}, y^* = y'e^{\varepsilon\alpha_2}, \psi^* = \psi e^{\varepsilon\alpha_3}, w^* = w'e^{\varepsilon\alpha_4}, \theta^* = \theta e^{\varepsilon\alpha_5} \text{ and } \phi^* = \phi e^{\varepsilon\alpha_6} \quad (20)$$

199 Here,  $\varepsilon (\neq 0)$  is the parameter of the group and  $\alpha$ 's are arbitrary real numbers whose  
200 interrelationship will be determined by our analysis. Equations (20) may be considered as a  
201 point transformation which transforms the coordinates  $(x', y', \psi, w', \theta, \phi)$  to the coordinates  
202  $(x^*, y^*, \psi^*, w^*, \theta^*, \phi^*)$ .

203 The system will remain invariant under the group transformation  $G_1$ , so the following  
204 relations among the exponents are obtained from equations (15) to (18),

$$205 \quad \left. \begin{aligned} \alpha_1 + 2\alpha_2 - 2\alpha_3 = 3\alpha_2 - \alpha_3 = -\alpha_4 = \alpha_2 - \alpha_3 = -\alpha_5 = -\alpha_6 \\ \alpha_1 + \alpha_2 - \alpha_3 - \alpha_4 = 2\alpha_2 - \alpha_4 = \alpha_2 - \alpha_3 = -\alpha_4 \\ \alpha_1 + \alpha_2 - \alpha_3 - \alpha_5 = 2\alpha_2 - \alpha_5 = 2\alpha_2 - 2\alpha_5 = 4\alpha_2 - 2\alpha_3 \\ \alpha_1 + \alpha_2 - \alpha_3 - \alpha_6 = 2\alpha_2 - \alpha_6 = -n\alpha_6 \end{aligned} \right\} \quad (21)$$

206 Again, the following relations are obtained from the boundary conditions (19),

$$207 \quad \begin{aligned} \alpha_2 = \alpha_3 \\ \alpha_5 = \alpha_6 = 0 \end{aligned} \quad (22)$$

208 Solving the system of linear equations (21) and (22), the following relationship are obtained,

209  $\alpha_1 = 2\alpha_2 = 2\alpha_3, \alpha_4 = \alpha_5 = \alpha_6 = 0$

210 by using the above relation the equation (20) reduces to the following group of  
211 transformation

212  $x^* = x'e^{2\varepsilon\alpha_2}, y^* = y'e^{\varepsilon\alpha_2}, \psi^* = \psi e^{\varepsilon\alpha_2}, w^* = w', \theta^* = \theta, \varphi^* = \varphi$  (23)

213 expanding equation (23) by Taylor's method in powers of  $\varepsilon$  and keeping terms up to the  
214 order  $\varepsilon$ , we have

215  $x^* - x' = 2\varepsilon x' \alpha_2, y^* - y' = \varepsilon y' \alpha_2, \psi^* - \psi = \varepsilon \psi \alpha_2, w^* - w' = 0, \theta^* - \theta = 0, \varphi^* - \varphi = 0$

216 In terms of differentials

217  $\frac{dx'}{2\alpha_2 x'} = \frac{dy'}{\alpha_2 y'} = \frac{d\psi}{\alpha_2 \psi} = \frac{dw'}{0} = \frac{d\theta}{0} = \frac{d\varphi}{0}$  (24)

218 Solving the equation (24) the following similarity variables are introduced,

219  $\eta = \frac{y'}{\sqrt{x'}}, \psi = \sqrt{x'} f(\eta), w' = g_0(\eta), \theta = \theta(\eta)$  and  $\varphi = \varphi(\eta)$

220 By using the above mentioned variables, equations (15), (16), (17) and (18) becomes

221  $f''' + \frac{1}{2} f f'' - M f'^2 + 2R' g_0 - \gamma f' + G_r \theta \cos \beta + G_m \varphi \cos \beta = 0$  (25)

222  $g_0'' + \frac{1}{2} f g_0' - 2R' f' - \gamma g_0 - M f' g_0 = 0$  (26)

223  $\frac{1}{P_r} (1 + T_c \theta + R) \theta'' + \frac{1}{P_r} T_c \theta'^2 + \frac{1}{2} f \theta' + Q \theta + E_c f''^2 = 0$  (27)

224  $\frac{1}{S_c} \varphi'' + \frac{1}{2} f \varphi' - \lambda \varphi^n = 0$  (28)

225 The corresponding boundary conditions (19) become

226  $\left. \begin{aligned} f' = 1, f = 0, g_0 = 0, \theta = 1, \varphi = 1 \text{ at } \eta = 0 \\ f' \rightarrow 0, g_0 \rightarrow 0, \theta \rightarrow 0, \varphi \rightarrow 0 \text{ as } \eta \rightarrow \infty \end{aligned} \right\}$  (29)

227 where primes denote differentiation with respect to  $\eta$  only and the parameters are defined as

228  $M = \frac{\sigma_0 B_0^2}{\rho}$  is the magnetic parameter

229  $\gamma = \frac{v^2 x'}{K U^2}$  is the porosity parameter

230  $R' = \frac{\Omega v x'}{U^2}$  is the rotational parameter

231  $G_r = \frac{g \beta_T (T_w - T_\infty) v x'}{U^3}$  is the Grashof number

232  $G_m = \frac{g \beta_c (C_w - C_\infty) v x'}{U^3}$  is the modified Grashof number

233  $T_c = c(T_w - T_\infty)$  is the thermal conductivity parameter

234  $P_r = \frac{\nu}{\alpha}$  is the Prandtl number

235  $R = \frac{16\sigma_s T_\infty^3}{3\kappa^* k_\infty}$  is the radiation parameter

236  $Q = \frac{Q_0 \nu}{\rho C_p U^2}$  is the heat source parameter

237  $E_c = \frac{U^2}{C_p (T_w - T_\infty)}$  is Eckert number

238  $S_c = \frac{\nu}{D_m}$  is the Schmidt number

239  $\lambda = \frac{k_0 (C_w - C_\infty)^{n-1} \nu}{U^2}$  is the reaction parameter

240 and  $n$  (integer) is the order of chemical reaction

241

## 242 **2.2 SKIN-FRICTION COEFFICIENTS, NUSSELT AND SHERWOOD NUMBER**

243

244 The physical quantities of the skin-friction coefficients, the reduced Nusselt number and  
245 reduced Sherwood number are calculated respectively by the following equations,

246  $C_f (R_e)^{\frac{1}{2}} = -f''(0)$  (30)

247  $C_{g_0} (R_e)^{\frac{1}{2}} = -g'_0(0)$  (31)

248  $N_u (R_e)^{-\frac{1}{2}} = -\theta'(0)$  (32)

249  $S_h (R_e)^{-\frac{1}{2}} = -\phi'(0)$  (33)

250 where,  $R_e = \frac{Ux'}{\nu}$  is the Reynolds number.

251

## 252 **3. RESULTS AND DISCUSSION**

253

254 The heat and mass transfer problem associated with laminar flow past an inclined plate of a  
255 rotating system has been studied. In order to investigate the physical representation of the  
256 problem, the numerical values of primary velocity, secondary velocity, temperature and  
257 species concentration from equations (25), (26), (27) and (28) with the boundary layer have  
258 been computed for different parameters as the magnetic parameter ( $M$ ), the rotational  
259 parameter ( $R'$ ), the porosity parameter ( $\gamma$ ), the Grashof number ( $G_r$ ), the modified Grashof  
260 number ( $G_m$ ), the radiation parameter ( $R$ ), the Prandtl number ( $P_r$ ), the Eckert number  
261 ( $E_c$ ), the thermal conductivity parameter ( $T_c$ ), the heat source parameter ( $Q$ ), the Schmidt  
262 number ( $S_c$ ), the reaction parameter ( $\lambda$ ), the inclination angle ( $\beta$ ) and the order of chemical  
263 reaction ( $n$ ) respectively.

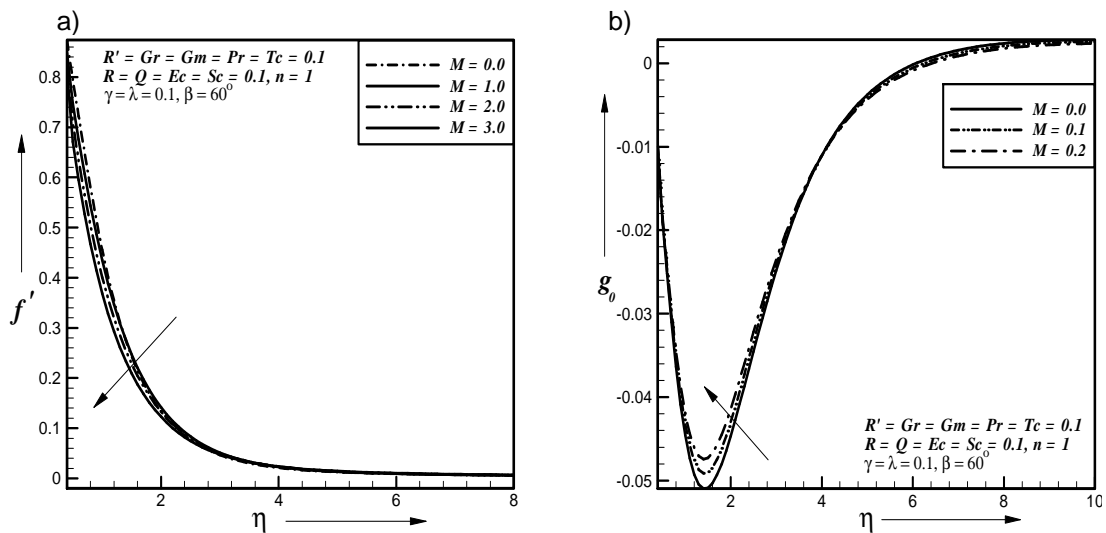
264 Figs. 2a and 2b show typical profiles for primary velocity ( $f'$ ) and secondary velocity ( $g_0$ ) for  
 265 different values of magnetic parameter, respectively. It is observed that as the magnetic  
 266 parameter increases, the primary and secondary velocities are decreases and increases  
 267 respectively, where other parameters have the value  $R' = Gr = Gm = \gamma = Pr = Tc = R = 0.1$ ,

268  $Q = Ec = Sc = \lambda = 0.1, \beta = 60^\circ, n = 1$ .

269 Figs. 3a, 3b, 3c and 3d present typical profiles for primary velocity ( $f'$ ), secondary  
 270 velocity ( $g_0$ ), temperature ( $\theta$ ) and concentration ( $\varphi$ ) for different values of rotational  
 271 parameter, respectively. It is observed that as the rotational parameter increases, the  
 272 primary velocity is decreases where as the secondary velocity, temperature and  
 273 concentration is increases respectively, where other parameters have the value

274  $M = Gr = Gm = \gamma = Pr = Tc = R = Q = Ec = Sc = 0.1, \lambda = 0.1, \beta = 60^\circ, n = 1$ .

275  
 276

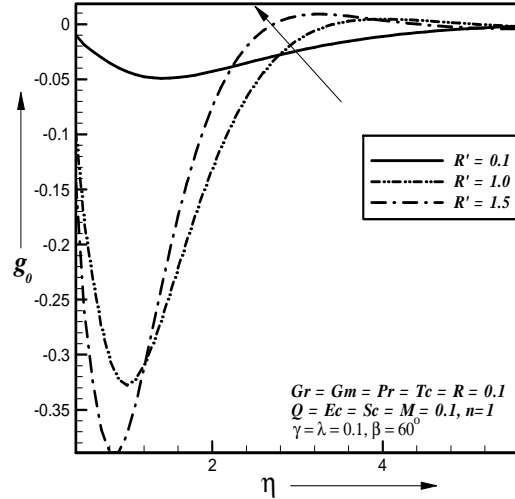
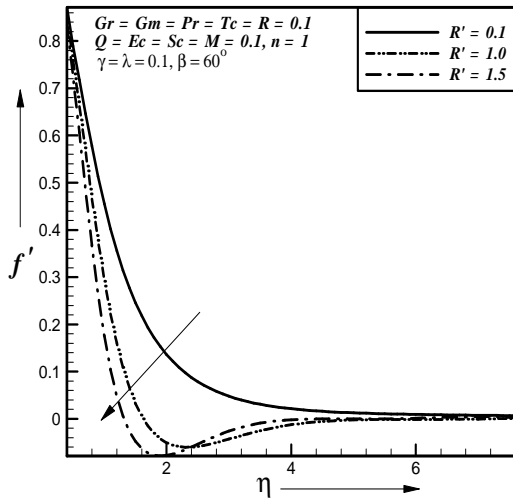


277  
 278  
 279  
 280  
 281  
 282  
 283

Fig. 2. Effect of magnetic parameter on a) primary velocity b) secondary velocity profiles

a)

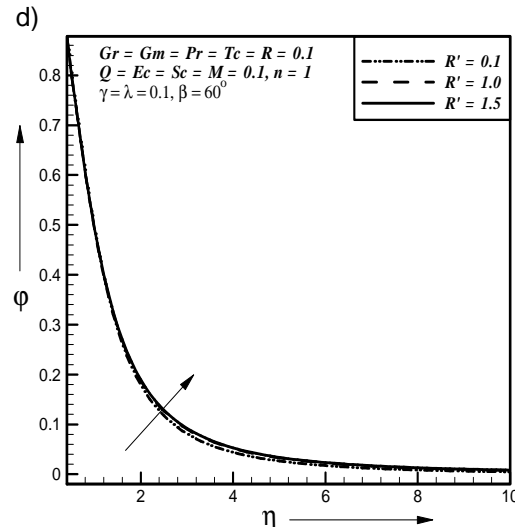
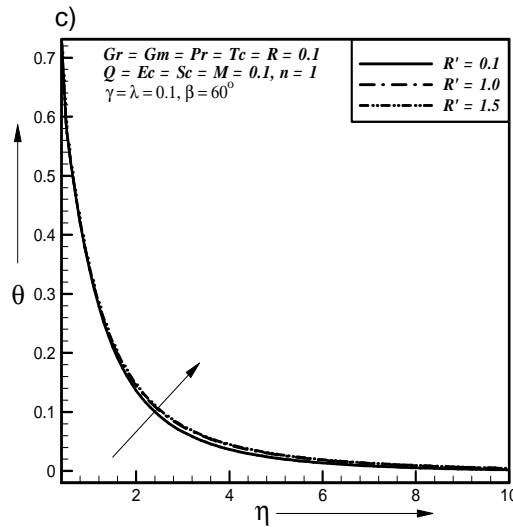
b)



284

285

286



287

288

289 **Fig. 3. Effect of rotational parameter on a) primary velocity b) secondary velocity c) temperature d) concentration profiles**

290

291

292 Figs. 4a, 4b, 4c and 4d show typical profiles for primary velocity ( $f'$ ), secondary velocity ( $g_0$ ), temperature ( $\theta$ ) and concentration ( $\phi$ ) for different values of porosity parameter  $\gamma$ , respectively. It is observed that as the porosity parameter increases, the primary velocity is decreases where as the secondary velocity, temperature and concentration is increases respectively, where other parameters have the value  $M = R' = Gr = Gm = Pr = Tc = R = Q = Ec = Sc = \lambda = 0.1, \beta = 60^\circ, n = 1$ .

293

294

295

296

297

298

299

300

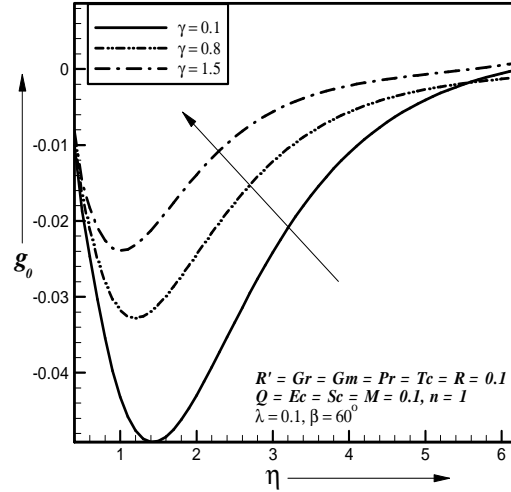
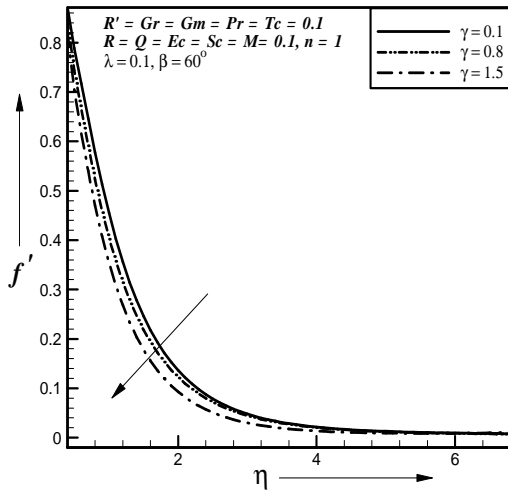
301

302

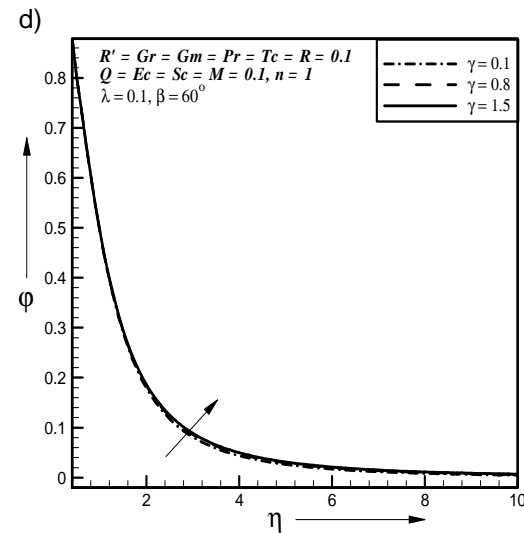
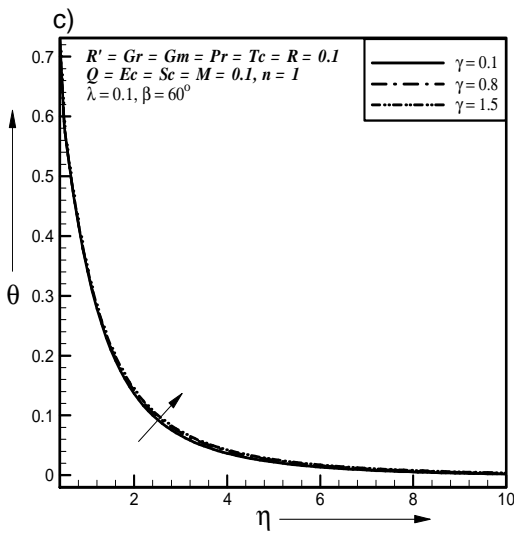
303

a)

b)



304  
305  
306



307  
308  
309  
310  
311

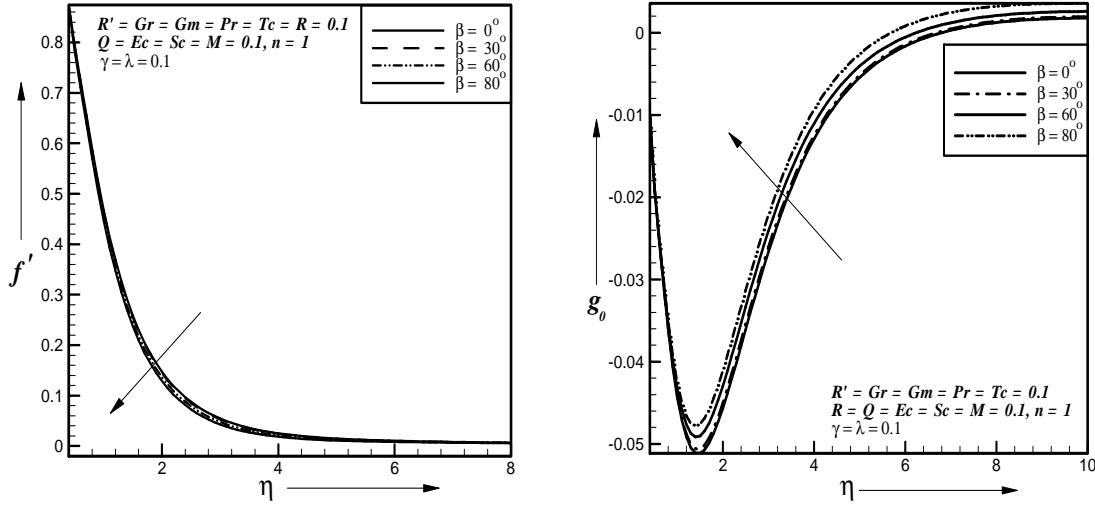
**Fig. 4. Effect of porosity parameter on a) primary velocity b) secondary velocity c) temperature d) concentration profiles**

312 Figs. 5a and 5b present typical profiles for primary velocity ( $f'$ ) and secondary  
313 velocity ( $g_0$ ) for different values of inclination angle, respectively. It is observed that as the  
314 inclination angle increases, the primary and secondary velocities are decreases and  
315 increases respectively, where other parameters have the value  $M = R' = Gr = Gm = \gamma = 0.1,$   
316  $Pr = Tc = R = Q = Ec = Sc = \lambda = 0.1, n = 1.$

317  
318  
319  
320  
321

a)

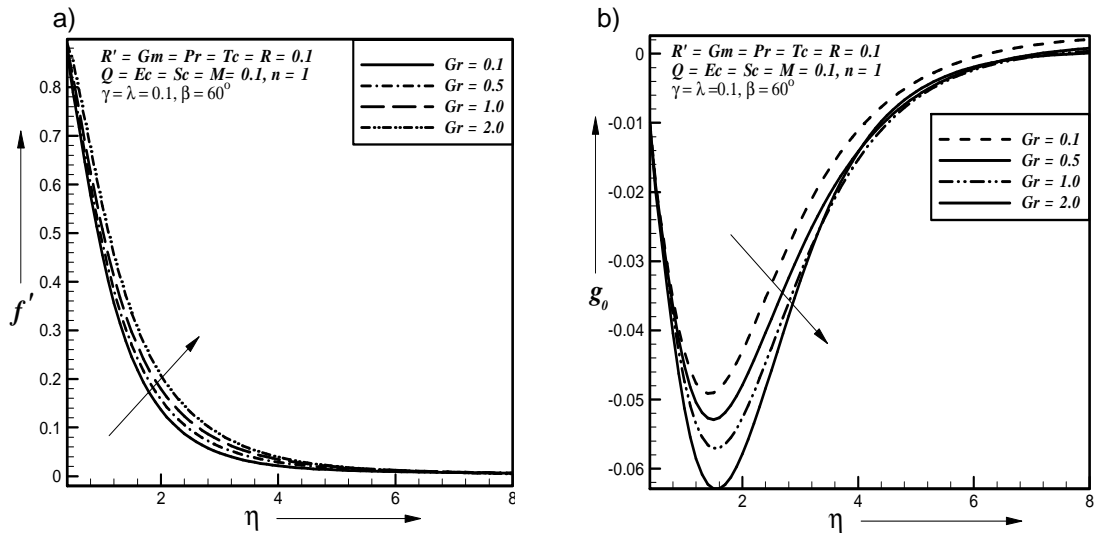
b)



322  
 323  
 324  
 325  
 326  
 327  
 328  
 329  
 330  
 331  
 332

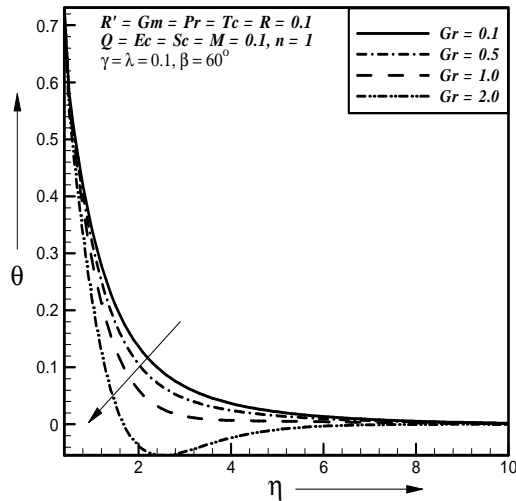
**Fig. 5. Effect of inclination angle on a) primary velocity b) secondary velocity profiles**

Figs. 6a, 6b and 6c present typical profiles for primary velocity ( $f'$ ), secondary velocity ( $g_0$ ) and temperature ( $\theta$ ) for different values of Grashof number, respectively. It is observed that as the Grashof number increases, the primary velocity is increases where as the secondary velocity and temperature is decreases respectively, where other parameters have the value  $M = R' = \gamma = Gm = Pr = Tc = R = Q = Ec = Sc = \lambda = 0.1, \beta = 60^\circ, n = 1$ .



333  
 334  
 335  
 336  
 337  
 338  
 339  
 340  
 341

c)



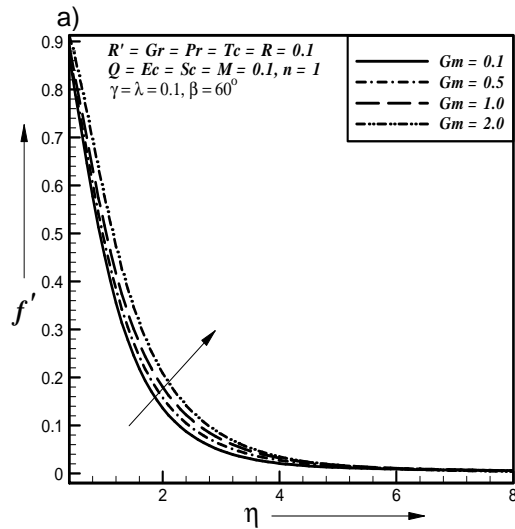
342  
343  
344  
345  
346

**Fig. 6. Effect of Grashof number on a) primary velocity b) secondary velocity c) temperature profiles**

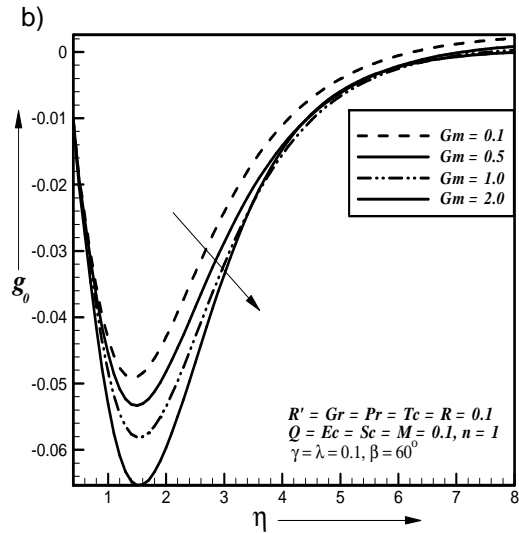
347 Figs. 7a, 7b and 7c show typical profiles for primary velocity ( $f'$ ), secondary velocity  
348 ( $g_0$ ) and concentration ( $\phi$ ) for different values of modified Grashof number, respectively. It  
349 is observed that as the modified Grashof number increases, the primary velocity is increases  
350 where as the secondary velocity and concentration is decreases respectively, where other  
351 parameters have the value  $M = R' = \gamma = Gr = Pr = Tc = R = Q = Ec = Sc = \lambda = 0.1, \beta = 60^\circ$ ,  
352  $n = 1$ .

353 Figs. 8a and 8b present typical profiles for primary velocity ( $f'$ ) and temperature ( $\theta$ ) for  
354 different values of Prandtl number, respectively. It is observed that as the Prandtl number  
355 increases, the primary velocity and temperature is increases and decreases respectively,  
356 where other parameters have the value  $M = R' = Gr = Gm = \gamma = Tc = R = Q = Ec = Sc = 0.1$ ,  
357  $\lambda = 0.1, \beta = 60^\circ, n = 1$ .

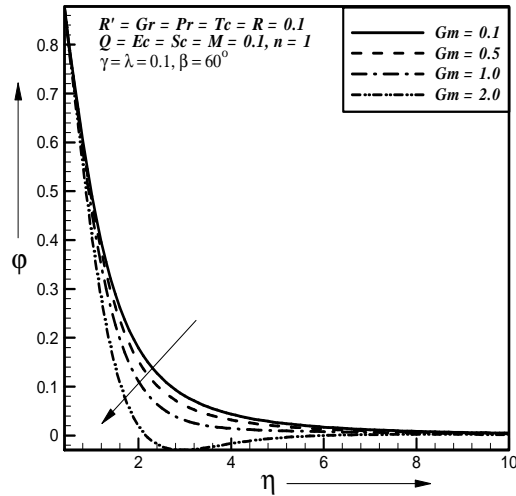
358



359  
360

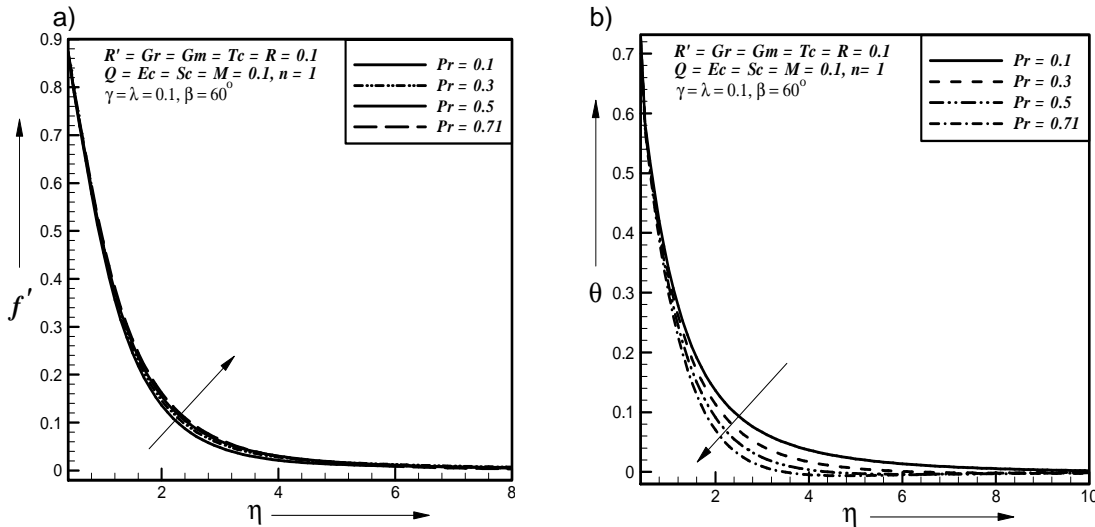


c)



361  
362  
363  
364  
365  
366

**Fig. 7. Effect of modified Grashof number on a) primary velocity b) secondary velocity c) concentration profiles**



367  
368  
369  
370

**Fig. 8. Effect of Prandtl number on a) primary velocity b) temperature profiles**

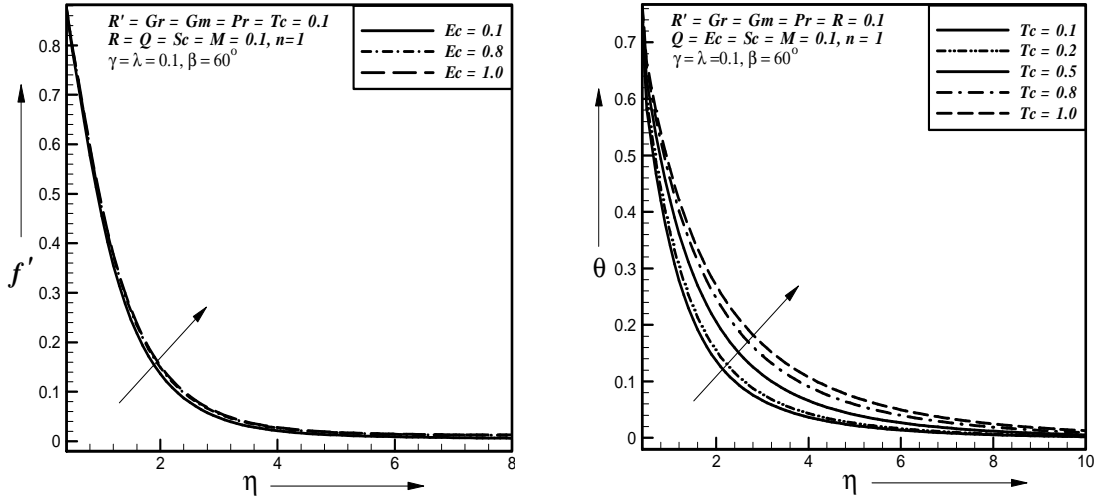
371 Fig. 9a displays typical profiles for primary velocity ( $f'$ ) for different values of Eckert number.  
372 It is observed that the primary velocity is increases with the increase of Eckert number,  
373 where other parameters have the value  $M = Gr = Gm = \gamma = Pr = Tc = R = Q = R' = Sc = 0.1$ ,  
374  $\lambda = 0.1, \beta = 60^0, n = 1$ .

375 Fig. 9b displays typical profiles for temperature ( $\theta$ ) for different values of Thermal  
376 conductivity parameter. It is observed that the temperature is increases with the increase of  
377 Thermal conductivity parameter, where other parameters have the value  
378  $M = Gr = Gm = \gamma = Pr = 0.1, Ec = R = Q = R' = Sc = \lambda = 0.1, \beta = 60^0, n = 1$ .

379  
380  
381

a)

b)



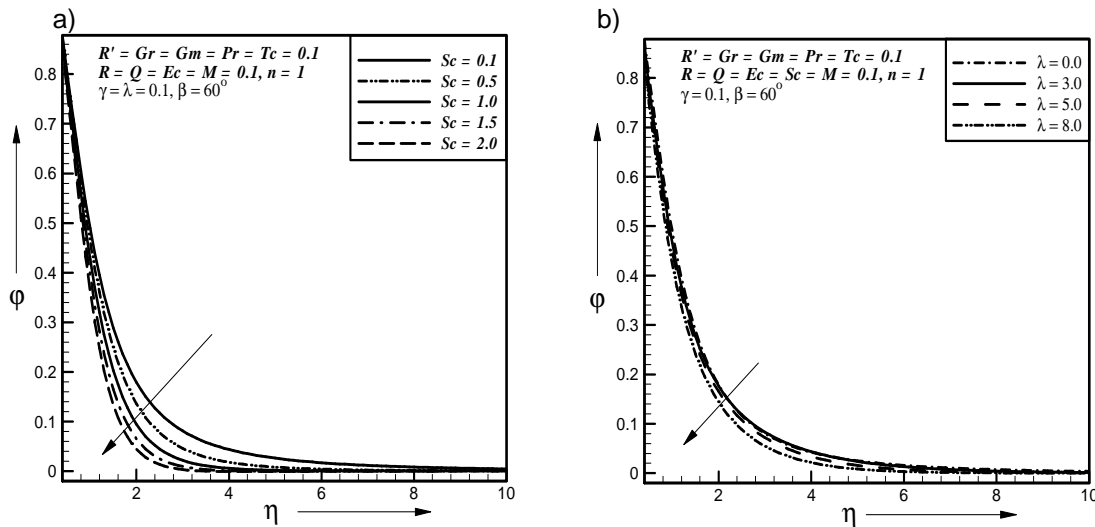
382  
383

384 **Fig. 9. Effect of a) Eckert number on primary velocity profiles b) thermal conductivity**  
385 **parameter on temperature profiles**

386 Fig. 10a represents typical profiles for concentration ( $\varphi$ ) for different values of Schmidt  
387 number  $Sc$ . It is observed that the concentration is decreases with the increase of Schmidt  
388 number, where other parameters have the value  $M = Gr = Gm = \gamma = Pr = Ec = Q = 0.1$ ,  
389  $Tc = R' = R = \lambda = 0.1, \beta = 60^\circ, n = 1$ .

390 Fig. 10b represents typical profiles for concentration ( $\varphi$ ) for different values of reaction  
391 parameter  $\lambda$ . The no reaction ( $\lambda = 0.0$ ) and destructive reaction ( $\lambda > 0.0$ ) is studied. It is  
392 observed that the concentration is decreases with the increase of reaction parameter, where  
393 other parameters have the value  $M = Gr = Gm = \gamma = Pr = Ec = Q = Tc = R' = R = Sc = 0.1$ ,  
394  $\beta = 60^\circ, n = 1$ .

395



396  
397  
398  
399

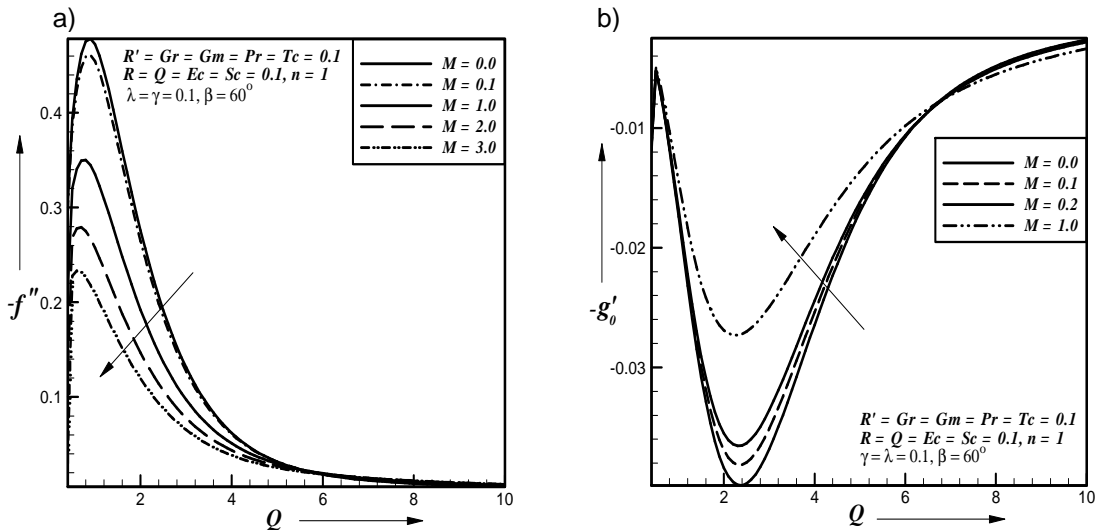
396 **Fig. 10. Effect of a) Schmidt number on concentration profiles b) reaction parameter**  
397 **on concentration profiles**

400 For the physical interest of the problem, the dimensionless skin-friction coefficient ( $-f''$ )  
 401 and ( $-g'_0$ ), the dimensionless heat transfer rate ( $-\theta'$ ) at the plate and the dimensionless  
 402 mass transfer rate ( $-\phi'$ ) at the plate are plotted against Heat source parameter ( $Q$ ) and  
 403 illustrated in Figs. 11-19.

404 Figs. 11a and 11b represent the primary shear stress ( $-f''$ ) and secondary shear stress  
 405 ( $-g'_0$ ) which are plotted against heat source parameter ( $Q$ ) for different values of magnetic  
 406 parameter. It is observed that the primary shear stress is decreases and secondary shear  
 407 stress is increases with the increase of magnetic parameter, where other parameters have  
 408 the value  $R' = Gr = Gm = \gamma = Pr = Ec = Q = Tc = R = Sc = \lambda = 0.1, \beta = 60^\circ, n = 1$ .

409 Figs. 12a and 12b represent the primary shear stress ( $-f''$ ) and secondary shear stress  
 410 ( $-g'_0$ ) which are plotted against heat source parameter ( $Q$ ) for different values of rotational  
 411 parameter. It is observed that the primary shear stress is decreases and secondary shear  
 412 stress is increases with the increase of rotational parameter, where other parameters have  
 413 the value  $M = Gr = Gm = \gamma = Pr = Ec = Q = Tc = R = Sc = \lambda = 0.1, \beta = 60^\circ, n = 1$ .

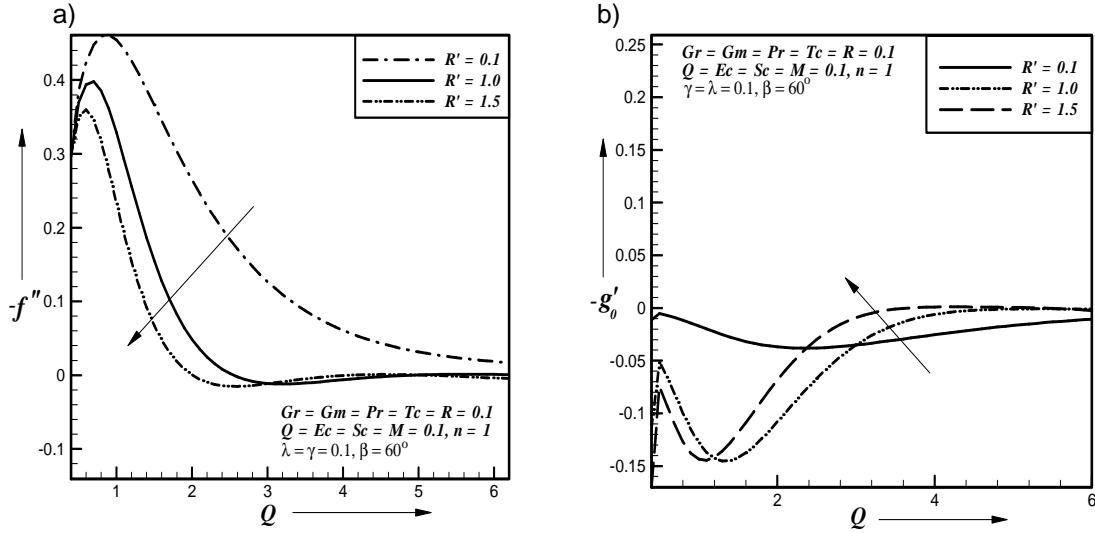
414  
 415



416  
 417  
 418  
 419  
 420  
 421  
 422  
 423  
 424  
 425  
 426  
 427  
 428  
 429  
 430  
 431  
 432

**Fig. 11. Effect of magnetic parameter on a) primary shear stress b) secondary shear stress**

433



434

435

436

437

438

439

440

441

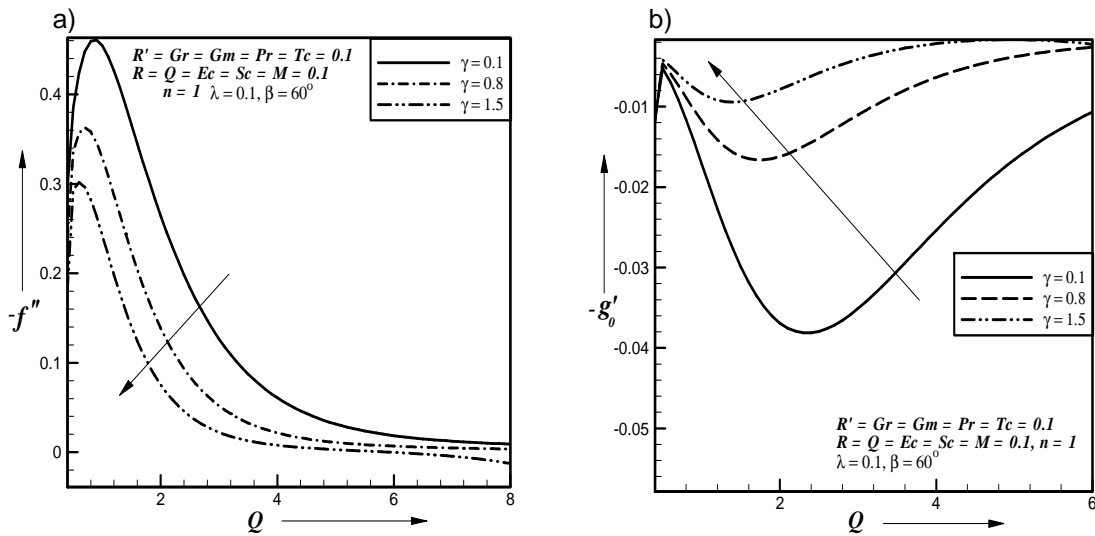
442

443

444

**Fig. 12. Effect of rotational parameter on a) primary shear stress b) secondary shear stress**

Figs. 13a and 13b represent the primary shear stress ( $-f''$ ) and secondary shear stress ( $-g'_0$ ) which are plotted against heat source parameter ( $Q$ ) for different values of porosity parameter. It is observed that the primary shear stress is decreases and secondary shear stress is increases with the increase of porosity parameter, where other parameters have the value  $M = Gr = Gm = R' = Pr = Ec = Q = Tc = R = Sc = \lambda = 0.1, \beta = 60^\circ, n = 1$ .



445

446

447

448

**Fig. 13. Effect of porosity parameter on a) primary b) secondary shear stress**

449

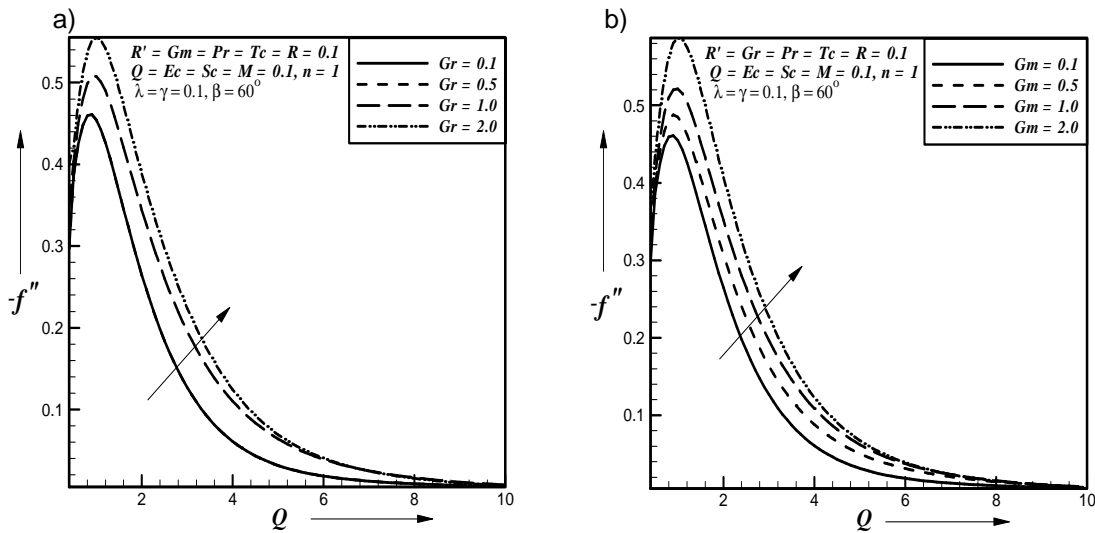
450

Fig. 14a represents the primary shear stress ( $-f''$ ) which is plotted against heat source parameter ( $Q$ ) for different values of Grashof number. It is observed that the primary shear

451 stress is increases with the increase of Grashof number, where other parameters have the  
 452 value  $M = \gamma = Gm = R' = Pr = Ec = Q = Tc = R = Sc = \lambda = 0.1, \beta = 60^0, n = 1$ .

453 Fig. 14b represents the primary shear stress ( $-f''$ ) which is plotted against heat source  
 454 parameter ( $Q$ ) for different values of modified Grashof number. It is observed that the  
 455 primary shear stress is increases with the increase of modified Grashof number, where other  
 456 parameters have the value  $M = \gamma = Gr = R' = Pr = Ec = Q = Tc = R = Sc = \lambda = 0.1, \beta = 60^0,$   
 457  $n = 1$ .

458  
 459



460  
 461  
 462  
 463

**Fig. 14. Effect of a) Grashof number b) modified Grashof on primary shear stress**

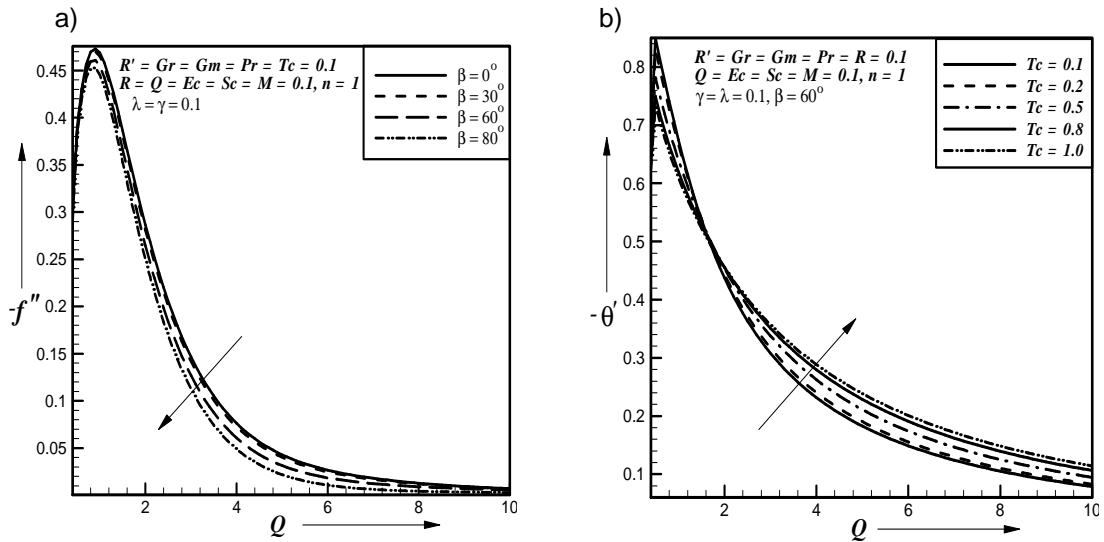
464 Fig. 15a represents the primary shear stress ( $-f''$ ) which is plotted against heat source  
 465 parameter ( $Q$ ) for different values of inclination angle. It is observed that the primary shear  
 466 stress is decreases with the increase of inclination angle, where other parameters have the  
 467 value  $M = \gamma = Gm = Gr = R' = Pr = Ec = Q = Tc = R = Sc = \lambda = 0.1, n = 1$ .

468 Fig. 15b represents the dimensionless heat transfer rate ( $-\theta'$ ) which is plotted against Heat  
 469 source parameter ( $Q$ ) for different values of thermal conductivity parameter. It is observed  
 470 that the heat transfer rate is increases with the increase of thermal conductivity parameter,  
 471 where other parameters have the value  $M = \gamma = Gm = Gr = R' = Pr = Ec = Q = R = Sc = 0.1,$   
 472  $\lambda = 0.1, \beta = 60^0, n = 1$ .

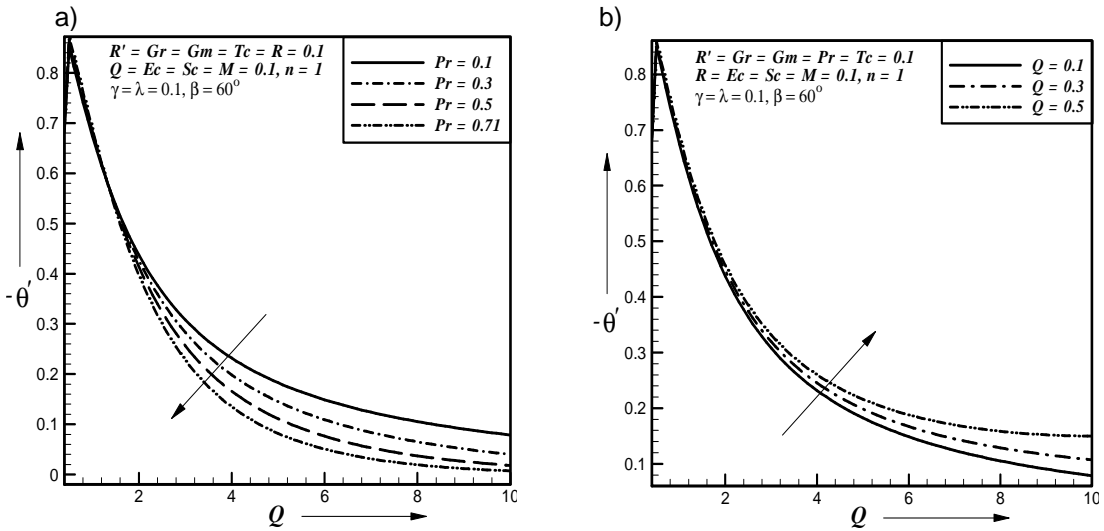
473 Fig. 16a represents the dimensionless heat transfer rate ( $-\theta'$ ) which is plotted against heat  
 474 source parameter ( $Q$ ) for different values of Prandtl number. It is observes that the heat  
 475 transfer rate is decreased with the increase of Prandtl number, where other parameters have  
 476 the value  $M = \gamma = Gm = Gr = R' = Tc = Ec = Q = R = Sc = \lambda = 0.1, \beta = 60^0, n = 1$ .

477 Fig. 16b represents the dimensionless heat transfer rate ( $-\theta'$ ) which is plotted against Heat  
 478 source parameter ( $Q$ ) for different values of heat source parameter. It is observed that the

479 heat transfer rate is increases with the increase of heat source parameter, where other  
 480 parameters have the value  $M = \gamma = Gm = Gr = R' = Tc = Ec = Pr = R = Sc = \lambda = 0.1, \beta = 60^0,$   
 481  $n = 1.$   
 482  
 483



484  
 485  
 486 **Fig. 15. Effect of a) inclination angle on primary shear stress b) thermal conductivity**  
 487 **parameter on heat transfer rate**  
 488  
 489



490  
 491  
 492 **Fig. 16. Effect of a) Prandtl number b) heat source parameter on heat transfer rate**  
 493

494 Fig. 17a represents the dimensionless heat transfer rate ( $-\theta'$ ) which is plotted against heat  
 495 source parameter ( $Q$ ) for different values of Eckert number. It is observed that the heat  
 496 transfer rate is increases with the increase of Eckert number, where other parameters have  
 497 the value  $M = \gamma = Gm = Gr = R' = Tc = Q = Pr = R = Sc = \lambda = 0.1, \beta = 60^0, n = 1.$

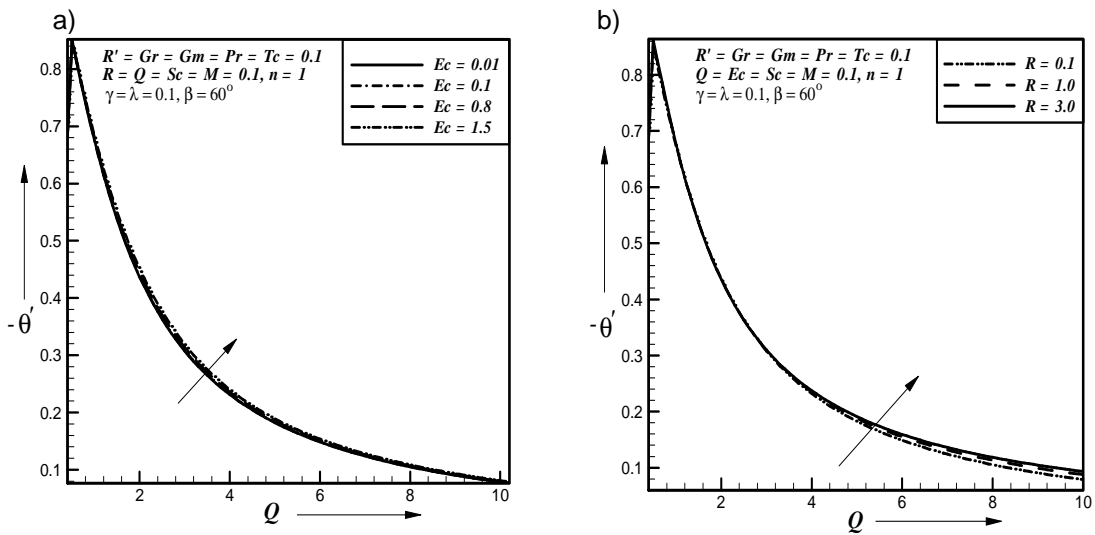
498 Fig. 17b represents the dimensionless heat transfer rate  $(-\theta')$  which is plotted against heat  
 499 source parameter  $(Q)$  for different values of radiation parameter. It is observed that the  
 500 heat transfer rate is increases with the increase of radiation parameter, where other  
 501 parameters have the value  $M = \gamma = Gm = Gr = R' = Tc = Q = Pr = Ec = Sc = \lambda = 0.1, \beta = 60^0,$   
 502  $n = 1.$

503 Fig. 18a represents the dimensionless mass transfer rate  $(-\phi')$  which is plotted against heat  
 504 source parameter  $(Q)$  for different values of Schmidt number. It is observed that the mass  
 505 transfer rate is decreases with the increase of Schmidt number, where other parameters  
 506 have the value  $M = \gamma = Gm = Gr = R' = Tc = Q = Pr = Ec = R = \lambda = 0.1, \beta = 60^0,$   
 507  $n = 1.$

508 Fig. 18b represents the dimensionless mass transfer rate  $(-\phi')$  which is plotted against heat  
 509 source parameter  $(Q)$  for different values of reaction parameter. It is observed that the  
 510 mass transfer rate is decreases with the increase of reaction parameter, where other  
 511 parameters have the value  $M = \gamma = Gm = Gr = R' = Tc = Q = Pr = Ec = R = Sc = 0.1, \beta = 60^0,$   
 512  $n = 1.$

513 Fig. 19 represents the dimensionless mass transfer rate  $(-\phi')$  which is plotted against heat  
 514 source parameter  $(Q)$  for different values of order of chemical reaction. It is observed that  
 515 the mass transfer rate is increases with the increase of order of chemical reaction, where  
 516 other parameters have the value  $M = \gamma = Gm = Gr = R' = Tc = Q = Pr = Ec = \lambda = R = Sc = 0.1,$   
 517  $\beta = 60^0.$

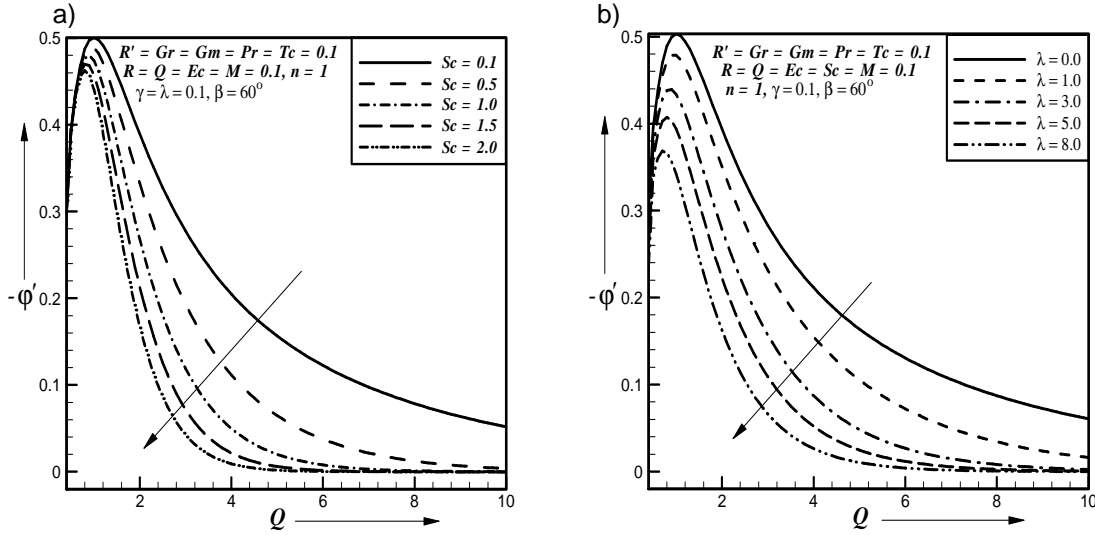
518  
 519



520  
 521  
 522  
 523  
 524  
 525  
 526  
 527  
 528

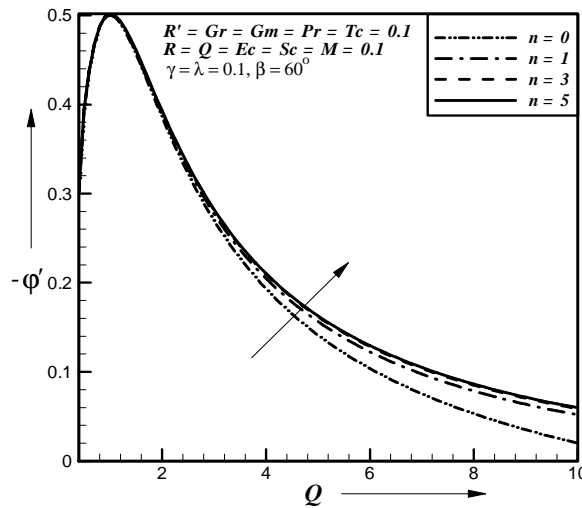
Fig. 17. Effect of a) Eckert number b) radiation parameter on heat transfer rate

529



530  
531  
532  
533  
534

Fig. 18. Effect of a) Schmidt number b) reaction parameter on mass transfer rate



535  
536  
537  
538  
539  
540  
541  
542  
543  
544  
545  
546  
547  
548  
549  
550

Fig. 19. Effect of order of chemical reaction on mass transfer rate

#### 4. CONCLUSION

Laminar boundary layer flow past an inclined permeable plate of a rotating system with the influence of magnetic field, thermal radiation and chemical reaction has been investigated. The results are presented for various parameters. The velocity, temperature and concentration distributions for different parameters are shown graphically. The important findings of the investigation from graphical representation are listed below:

The primary velocity profiles are decreases due to increase of magnetic parameter where as the reverse effect is found for the secondary velocity profiles. Also the primary shear stress is decreases due to increase of magnetic parameter where as the reverse effect is found for secondary shear stress.

551 The primary velocity profiles and primary shear stress are decreases due to increase of  
552 rotational parameter where as the reverse effect is found for the secondary velocity profiles  
553 and secondary shear stress. Also the temperature and concentration boundary layer  
554 thickness are increases due to increase of rotational parameter.

555 The primary velocity profiles and primary shear stress are decreases due to increase of  
556 permeability of the porous medium where as the reverse effect is found for the secondary  
557 velocity profiles and secondary shear stress. Also the temperature and concentration  
558 boundary layer thickness are increases due to increase of permeability of the porous  
559 medium.

560 The primary velocity profiles and primary shear stress are decreases due to increase of  
561 inclination angle where as the reverse effect is found for the secondary velocity profiles.

562 The primary velocity profiles and primary shear stress are increases due to increase of  
563 Grashof number where as the reverse effect is found for the secondary velocity profiles. Also  
564 the temperature boundary layer thickness is decreases due to increase of Grashof number.

565 The primary velocity profiles and primary shear stress are increases due to increase of  
566 modified Grashof number where as the reverse effect is found for the secondary velocity  
567 profiles. Also the concentration boundary layer thickness is decreases due to increase of  
568 modified Grashof number.

569 The primary velocity profiles are increases due to increase of Prandtl number. The thermal  
570 boundary layer thickness as well as the heat transfer rate at the plate is decreases as the  
571 Prandtl number increases.

572 The heat transfer rate at the plate as well as the primary velocity is increases due to  
573 increase of Eckert number.

574 The temperature boundary layer thickness as well as the heat transfer rate at the plate is  
575 increases due to increase of thermal conductivity parameter.

576 The heat transfer rate at the plate is increases due to increase of heat source parameter.

577 The heat transfer rate at the plate is increases due to increase of radiation parameter.

578 The concentration boundary layer thickness as well as the mass transfer rate at the plate is  
579 decreases due to increase of Schmidt number.

580 The concentration boundary layer thickness as well as the mass transfer rate at the plate is  
581 decreases due to no reaction and destructive reaction.

582 The mass transfer rate at the plate is increases due to increase of order of chemical  
583 reaction.

584

## 585 **COMPETING INTERESTS**

586

587 Authors have declared that no competing interests exist.

588

589

## 590 **REFERENCES**

591

592 1. Bluman GW, Kumei S. Symmetries and Differential Equations. Springer-verlag: New  
593 York; 1989.

594 2. Helmy KA. MHD boundary layer equations for power law fluids with variable electric  
595 conductivity. *Mechanica*. 1995;30:187-200.

596 3. Pakdemirli M, Yurusoy M. Similarity transformations for partial differential equations.  
597 *SIAM Review*. 1998;40:96-101.

- 598 4. Kalpakides VK, Balassas KB. Symmetry groups and similarity solutions for a free  
599 convective boundary-layer problem. *International Journal of Non-Linear Mechanics*.  
600 2004;39:1659-1670.
- 601 5. Makinde OD. Free convection flow with thermal radiation and mass transfer past moving  
602 vertical porous plate. *International Communications in Heat and Mass Transfer*. 2005  
603 ;32:1411-1419.
- 604 6. Seddeek MA, Salem AM. Laminar mixed convection adjacent to vertical continuously  
605 stretching sheet with variable viscosity and variable thermal diffusivity. *Heat and Mass*  
606 *Transfer*. 2005;41:1048-1055.
- 607 7. Ibrahim FS, Elaiw AM, Bakr AA. Effect of the chemical reaction and radiation absorption  
608 on the unsteady MHD free convection flow past a semi infinite vertical permeable  
609 moving plate with heat source and suction. *Communications in Nonlinear Science and*  
610 *Numerical Simulation*. 2008; 13:1056-1066.
- 611 8. El-Kabeir SMM, El-Hakiem MA, Rashad. Lie group analysis of unsteady MHD three  
612 dimensional dimensional by natural convection from an inclined stretching surface  
613 saturated porous medium. *Journal of Computational and Applied Mathematics*.  
614 2008;213:582-603.
- 615 9. Rajeswari R, Jothiram J, Nelson VK. Chemical Reaction, Heat and Mass Transfer on  
616 Nonlinear MHD Boundary Layer Flow through a Vertical Porous Surface in the Presence  
617 of Suction. *Applied Mathematical Sciences*. 2009;3:2469-2480.
- 618 10. Chandrakala P. Chemical Reaction Effects on MHD Flow Past An Impulsively Started  
619 Semi-Infinite Vertical Plate. *International Journal of Dynamics of Fluids*. 2010;6:77-79.
- 620 11. Joneidi AA, Domairry G, Balaelahi M. Analytical treatment of MHD free convective flow  
621 and mass transfer over a stretching sheet with chemical reaction. *Journal of the Taiwan*  
622 *Institute of Chemical Engineers*. 2010;41: 35-43.
- 623 12. Muhaimin, Kandasamy R, Hashim I. Effect of chemical reaction, heat and mass transfer  
624 on nonlinear boundary layer past a porous shrinking sheet in the presence of suction.  
625 *Nuclear Engineering and Design*. 2010;240(5):933-939.
- 626 13. Rahman MM, Salahuddin KM. Study of hydromagnetic heat and mass transfer flow over  
627 an inclined heated surface with variable viscosity and electric conductivity.  
628 *Communications in Nonlinear Science and Numerical Simulation*. 2010;15:2073-2085.